# Evaluation of task-specific ionic liquids applied as pervaporation membranes: experimental and COSMO-RS studies

Xiao Xu [a,b], GillesVan Eygen [a, b, c], Cristhian Molina-Fernández [a, b], Daria Nikolaeva [a,b], Ysaline Depasse [a, b], Sara Chergaoui [a,b,] Yusak Hartanto [a,b], Bart Van der Bruggena [c], João A.P. Coutinho [d], Anita Buekenhoudt [e], Patricia Luis [a,b]

[a] *Institute of Mechanics, Materials and Civil Engineering - Materials & Process Engineering (iMMC-IMAP), UCLouvain, Place Sainte Barbe 2, 1348 Louvain-la-Neuve, Belgium*

[b] *Research & Innovation Centre for Process Engineering (ReCIPE), Place Sainte Barbe, 2 bte L5.02.02 - B-1348 Louvain-la-Neuve (Belgium)*

[c] *Process Engineering for Sustainable Systems (ProcESS), Katholieke Universiteit Leuven, Celestijnenlaan 200f, 3001 Leuven, Belgium*

[d] *CICECO-Aveiro Institute of Materials, Chemistry Department, University of Aveiro, 3810-193 Aveiro, Portugal*

[e] *Unit Separation and Conversion Technology, Vlaamse Instelling voor Technologisch Onderzoek (VITO NV), Boeretang 200, 2400 Mol, Belgium*

Corresponding authors: xiao.xu@uclouvain.be

patricia.luis@uclouvain.be

## 1. Characterization of ILs

### 1.1. NMR characterization

NMR samples were prepared by adding 0.5 mL of $CDCl_3$ to ~30 mg of ionic liquid into 5 mm NMR tubes. $^1H$ and $^{13}C$ NMR spectra were recorded at room temperature (295 K) on a Bruker Avance 500 spectrometer operating at 500.13 MHz for the proton-1H and 125.76 MHz for the carbon-13C. Experiments were run using a BBO {1H, X} probehead equipped with a z-gradient coil. $^1H$ and $^{13}C$ chemical shifts were referenced to the residual undeuterated $CDCl_3$ signal (7.26 ppm for $^1H$ and 77.16 ppm for $^{13}C$ NMR spectra). Standard zg programs were employed for 1D NMR experiments. A Waltz-16 decoupling scheme with a pulse of 80 µsec was used for $^{13}C\{^1H\}$ NMR analysis.

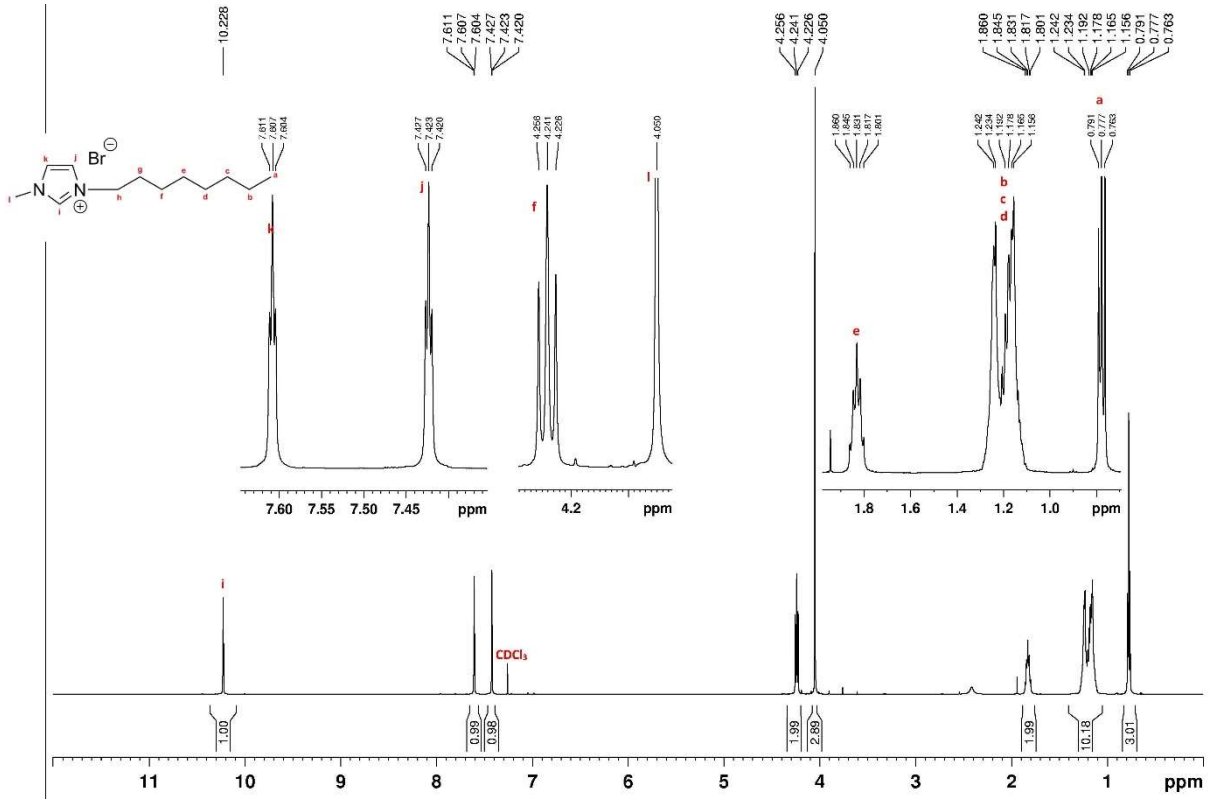


**Fig. S1**. $^1H$ NMR spectrum of [Omim][Br] in $CDCl_3$. Full spectrum.

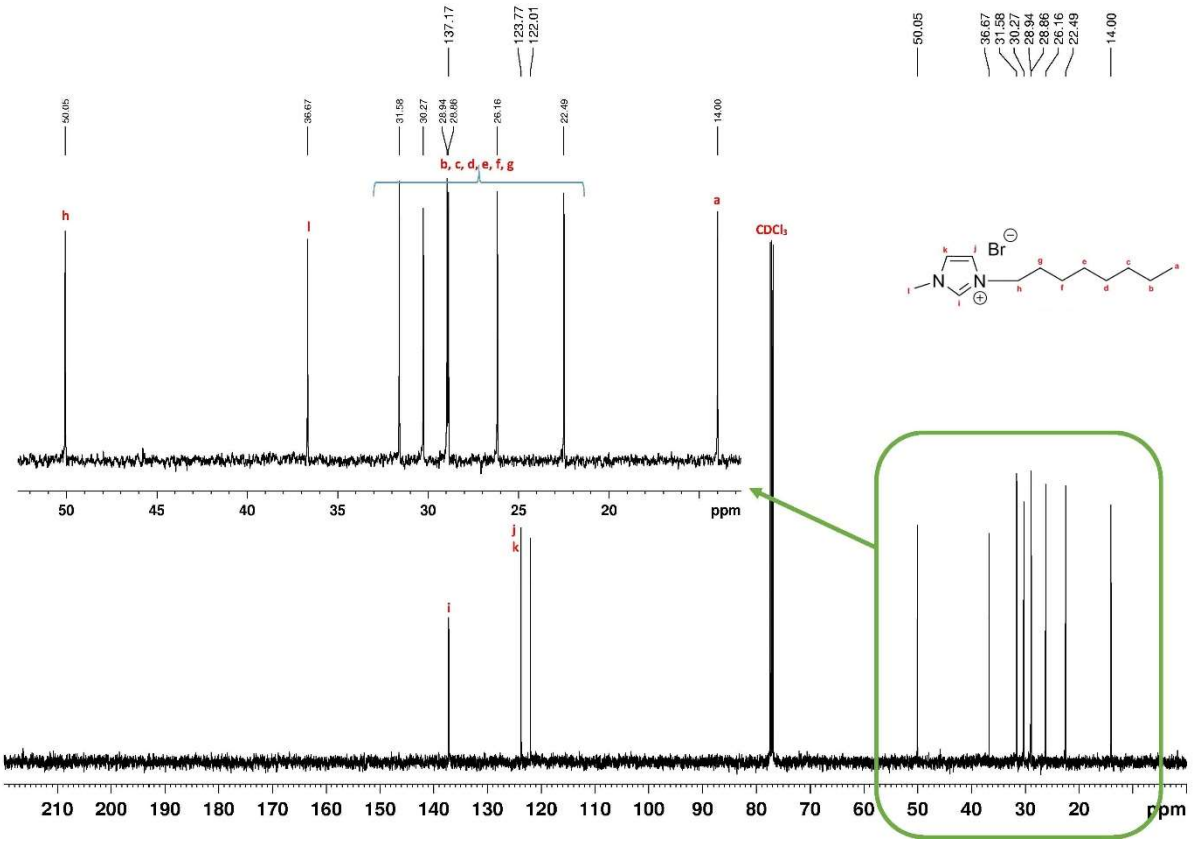


48

49 **Fig. S2**. $^{13}C\{^{1}H\}$ NMR spectrum of [Omim][Br] in $CDCl_3$. Full spectrum.

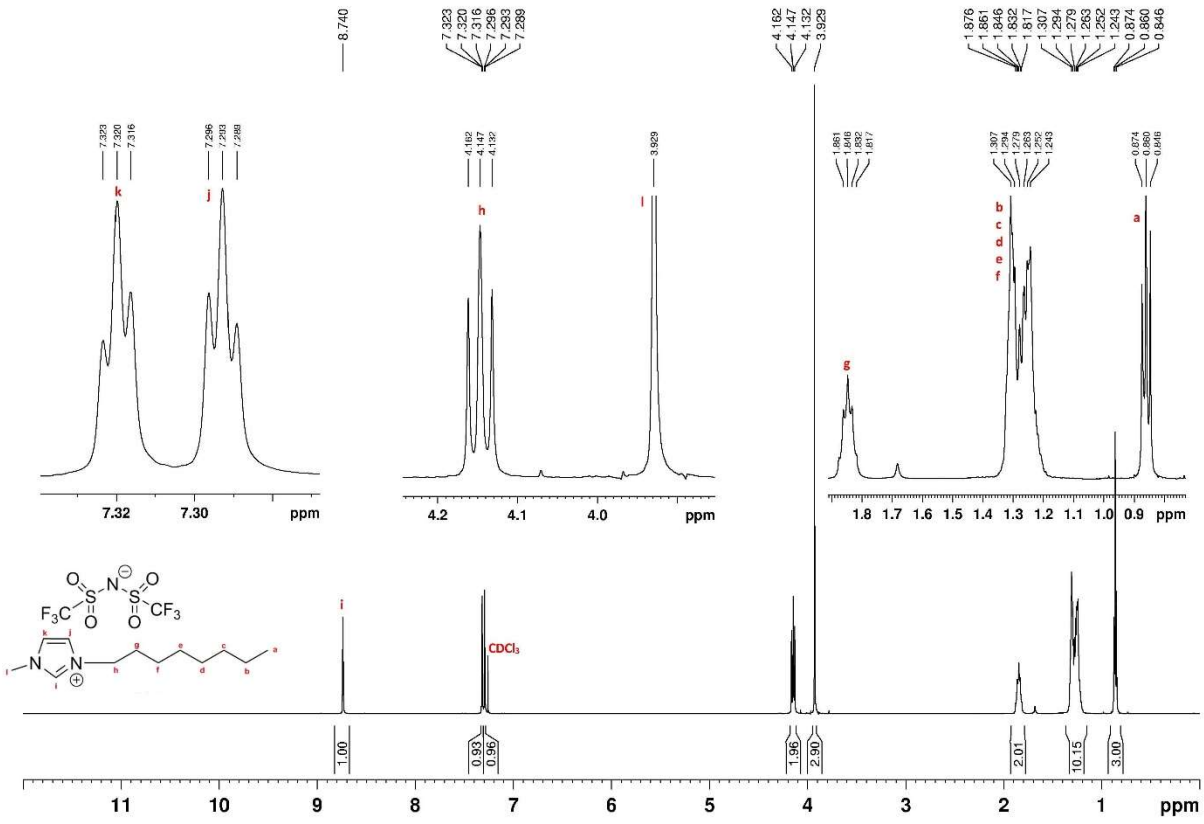

**Fig. S3**. $^{1}H$ NMR spectrum of [Omim][NTf2] in $CDCl_3$. Full spectrum.

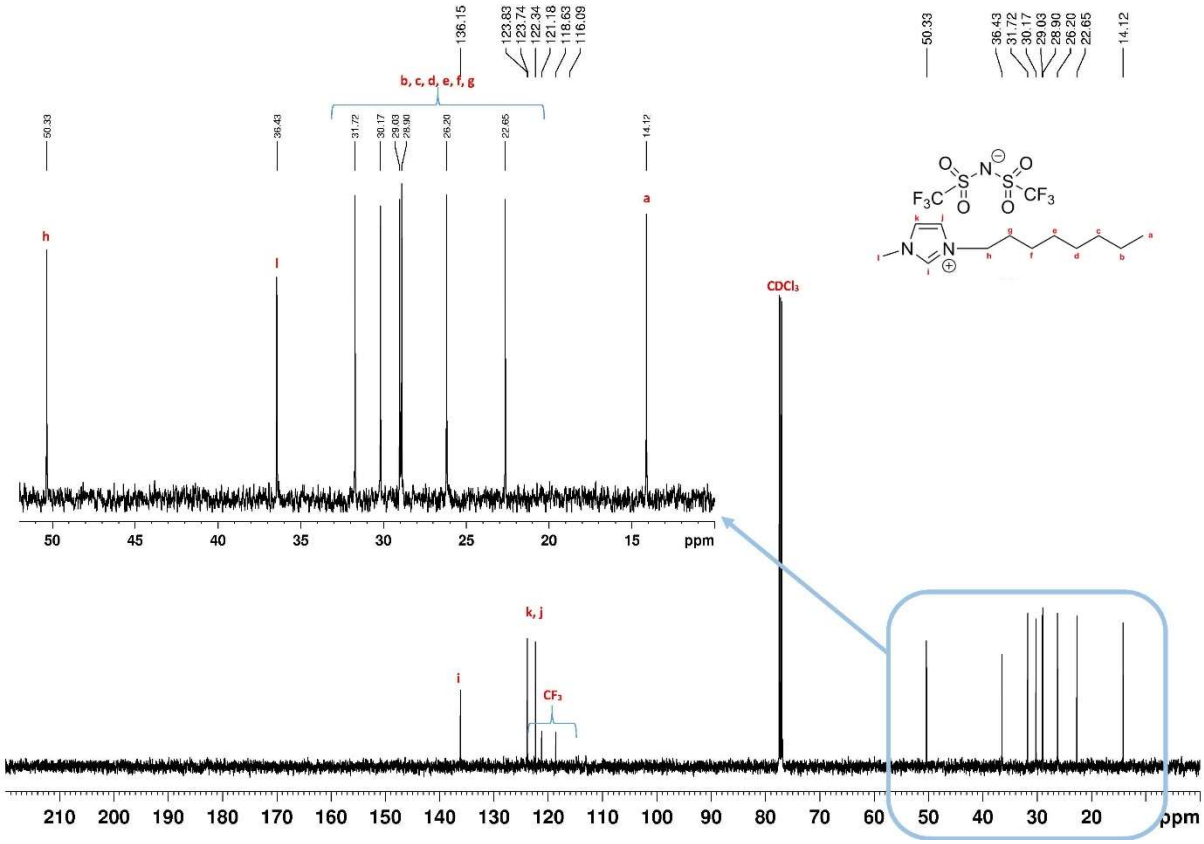


**Fig. S4**. $^{13}C\{^{1}H\}$ NMR spectrum of [Omim][NTf2] in $CDCl_3$. Full spectrum.

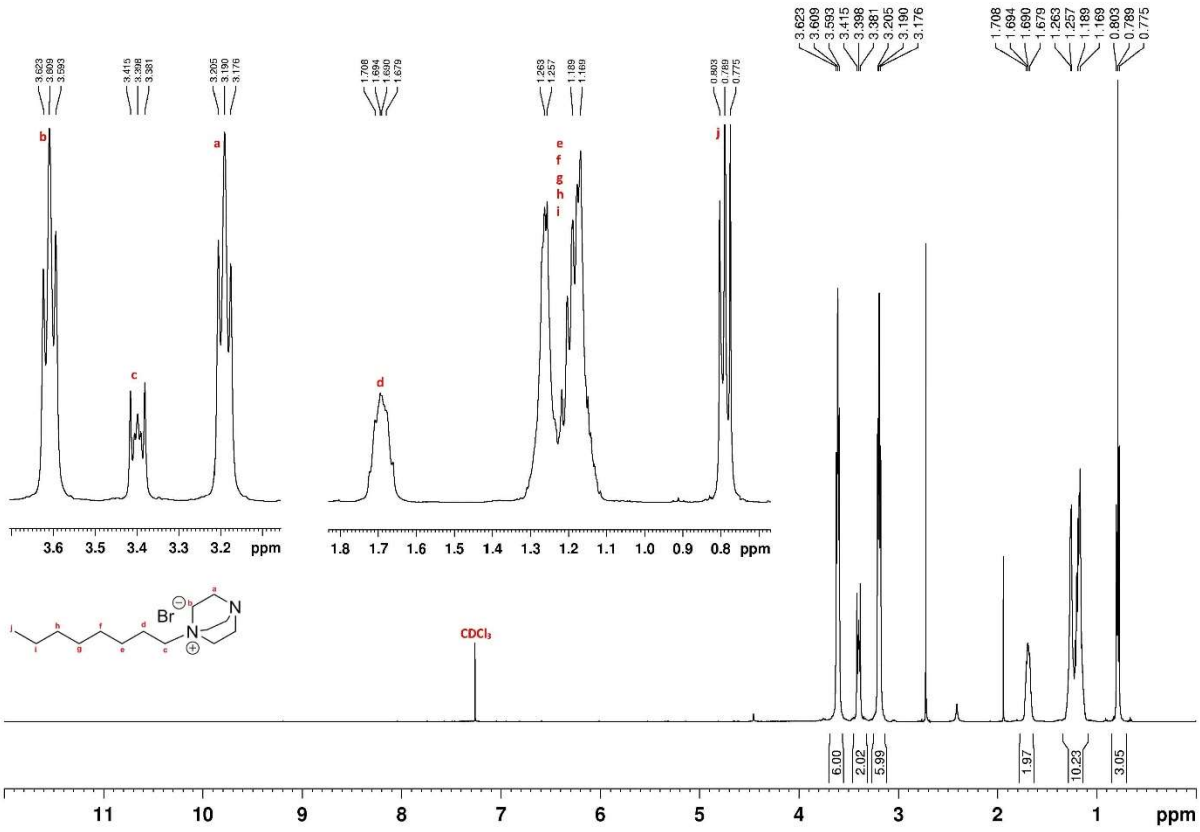


54 **Fig. S5**. $^{1}$H NMR spectrum of [ODABCO][Br] in $CDCl_3$. Full spectrum.

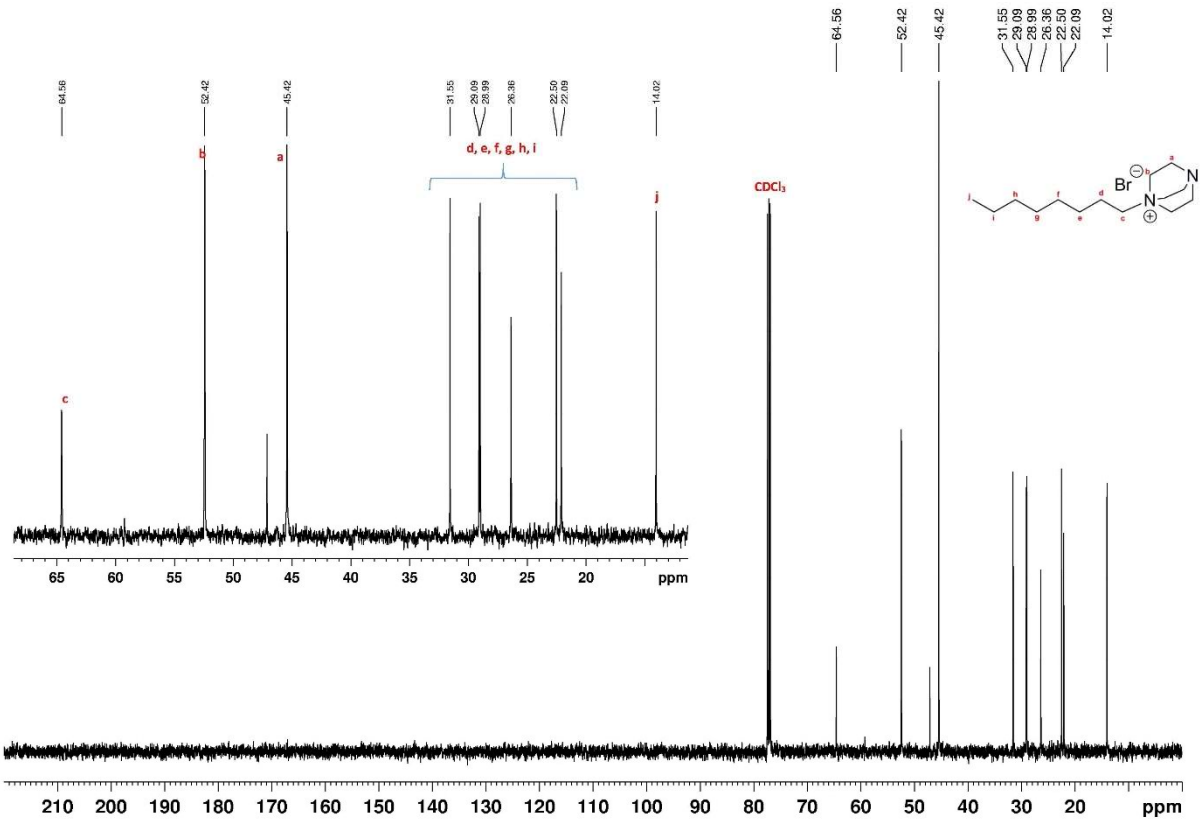


55

56 **Fig. S6**. $^{13}C\{^{1}H\}$ NMR spectrum of [ODABCO][Br]in $CDCl_3$. Full spectrum.

## 1.2 FTIR characterization

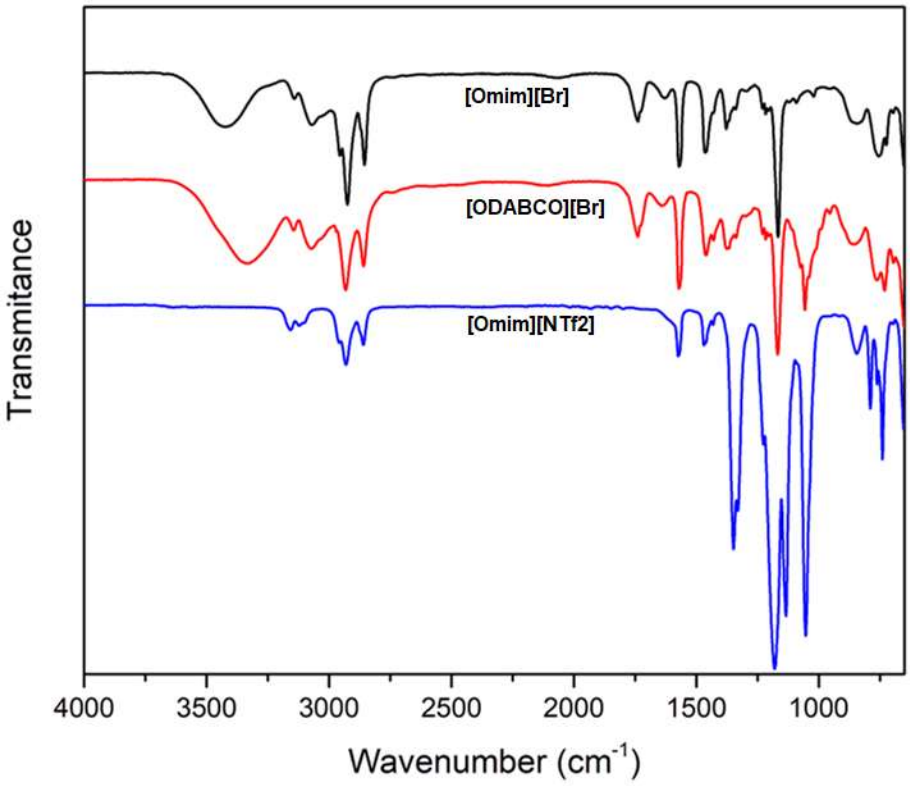


**Fig. S7**. FTIR spectrum of ILs.

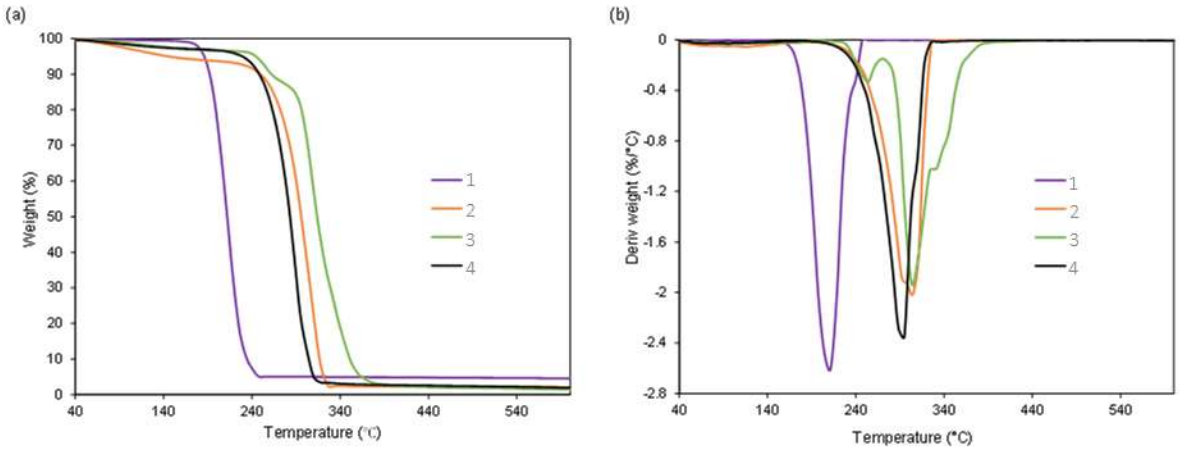


**Fig. S8**. (a) TGA curves and (b) DTGA curves of ILs (1: [TBA][Br], 2: [Omim][Br], 3: [ODABCO][Br], and 4: [Omim][NTf2]).

As observed in Fig. S8, [TBA][Br], [Omim][Br] and [Omim][NTf2] show only one sharp weight loss step with a maximum at 211, 304 and 294°C, respectively. It can be attributed that all the interactions of these three ILs collapse over critical temperatures, and ILs start decomposing [1]. As a consequence of the decomposition, over 90% weight losses are observed in the temperature range between 150-400°C. However, the thermal degradation of [ODABCO][Br] shows two steps of weight losses, the first small one with a maximum at 254 °C and then the second large one with a maximum at 302 °C. The small weight loss is due to the loss of alkyl chains, whereas the large loss with a maximum at 302°C results from the collapse of the all the stacking interactions of [ODABCO][Br] [2]. Importantly, the collapse of the stacking interaction occurs 83–93°C earlier for the aliphatic cation (tetrabutylammonium), when compared with the aromatic imidazolium cation (3-Methyl-1-octylimidazolium), and 91°C earlier when compared to the cyclic quaternary ammonium cation (1-octyl-1,4-diazabicyclo[2.2.2]octanium). It can be explained that there are π–π intermolecular interactions within [Omim][Br] and [Omim][NTf2] as well as anion–π interaction within [Omim][Br] [3, 4]. These interactions can stabilize the ILs. As for [ODABCO][Br], the presence of strained rings around the nitrogen atoms allows for a closer approach of bromide anion, resulting in the stronger interaction between them [5]. Therefore, it was concluded that a stronger interaction can lead to the higher collapse temperature of [ODABCO][Br]. Based on the TGA results, these 4 kinds of ILs can be feasible to be used for low-temperature pervaporation.

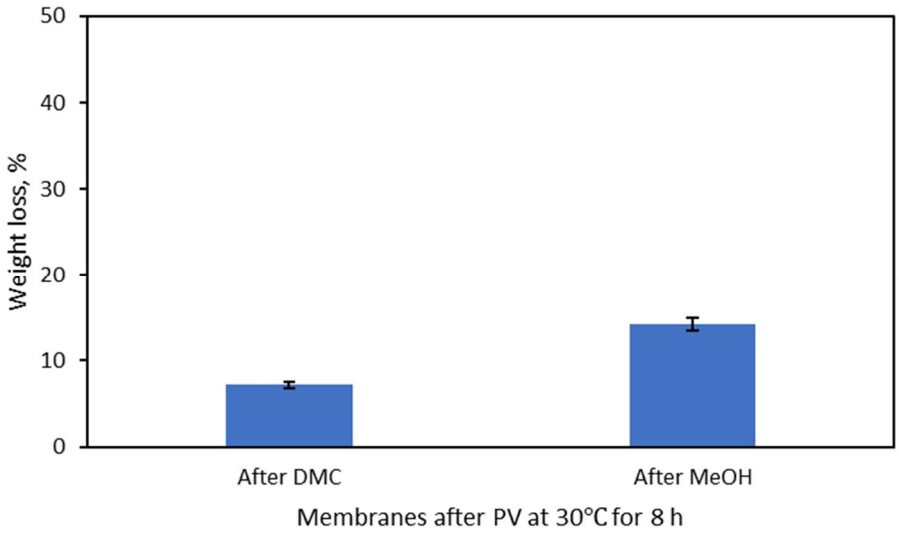


**Fig. S9**. Dynamic stability of [Omim][Br] after single solvent PV.

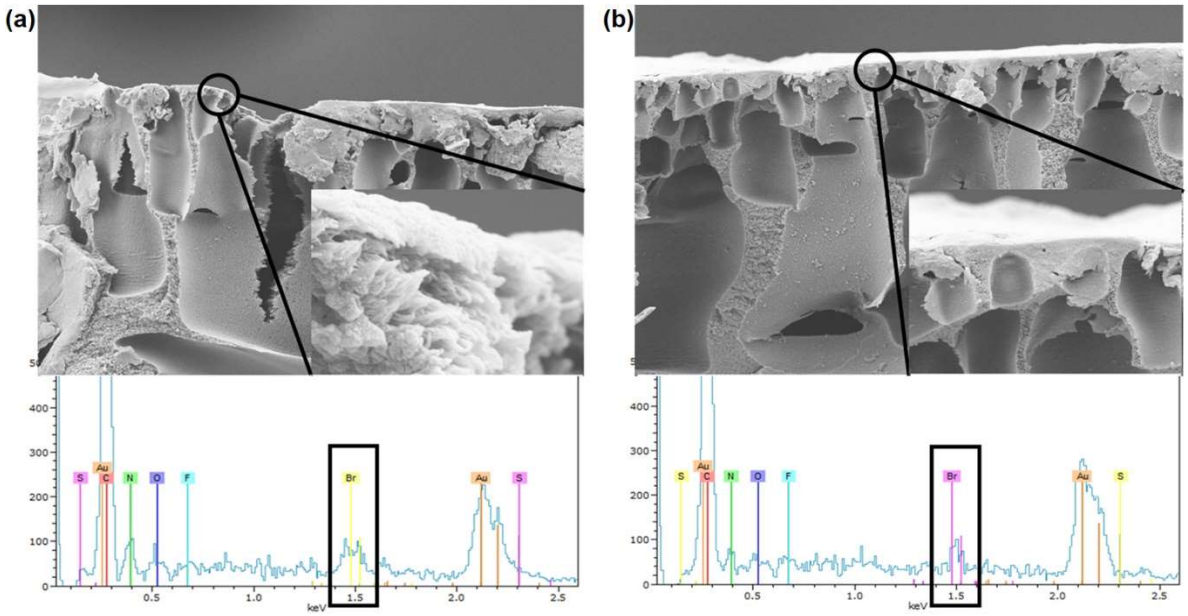


**Fig. S10**. SEM and EDS results of [Omim][Br]-based membranes after DMC (a), and MeOH (b) PV at 30℃ for 8 h.

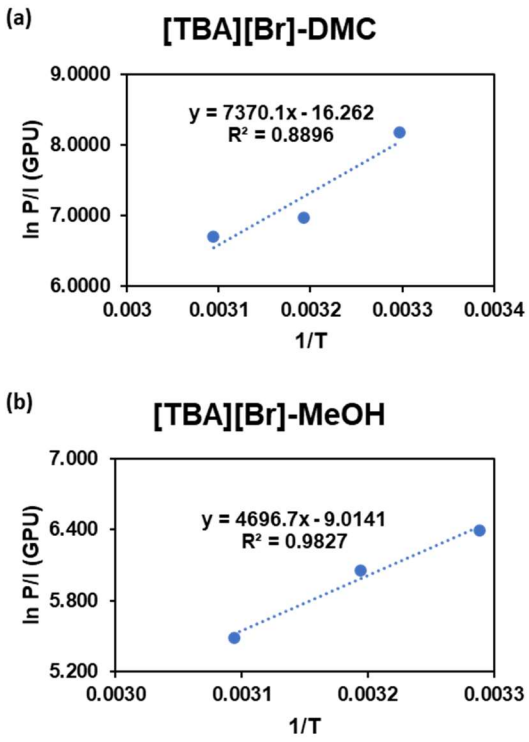


**Fig. S11**. Logarithmized permeance (a) DMC and (b) MeOH versus the inverse temperature to calculate the activation energy (slope in $J \cdot mol^{-1}$) for SILM of [TBA][Br].

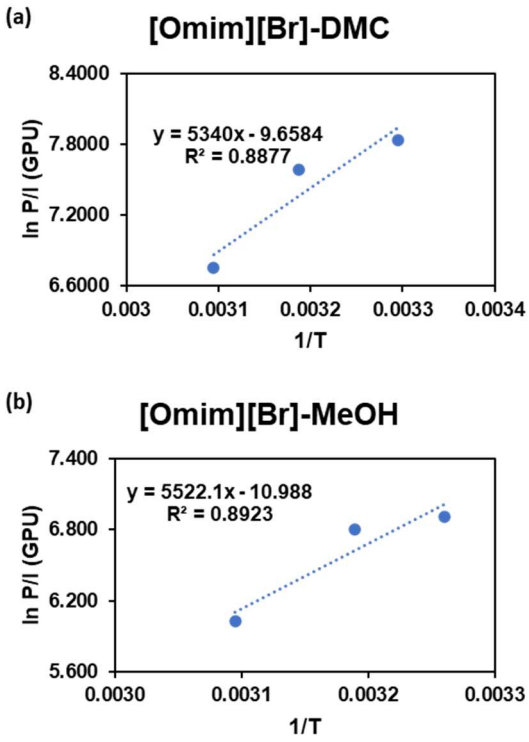


**Fig. S12**. Logarithmized permeance (a) DMC and (b) MeOH versus the inverse temperature to calculate the activation energy (slope in $J \cdot mol^{-1}$) for SILM of [Omim][Br].

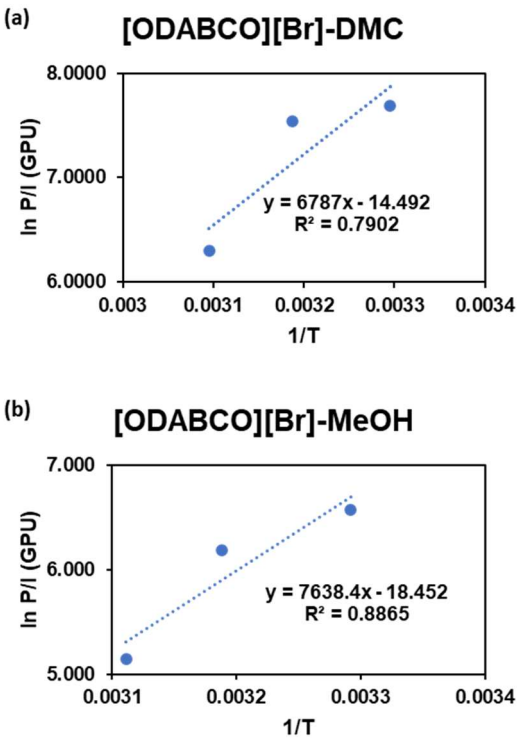


**Fig. S13**. Logarithmized permeance (a) DMC and (b) MeOH versus the inverse temperature to calculate the activation energy (slope in $J \cdot mol^{-1}$) for SILM of [ODABCO][Br].

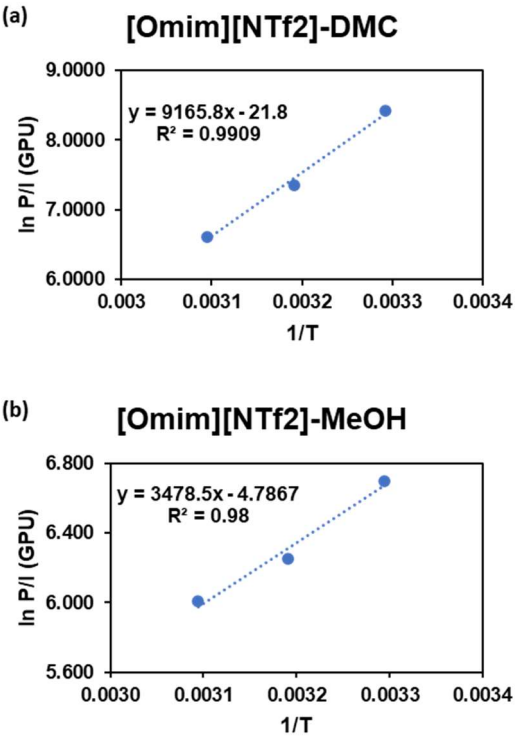


**Fig. S14**. Logarithmized permeance (a) DMC and (b) MeOH versus the inverse temperature to calculate the activation energy (slope in $J \cdot mol^{-1}$) for SILM of [Omim][NTf2].

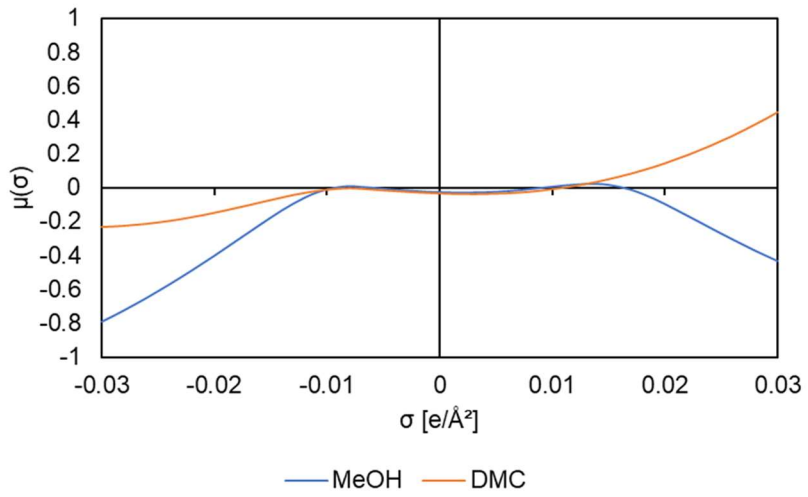


**Fig. S15**. $\sigma$-potentials of the considered solvents.

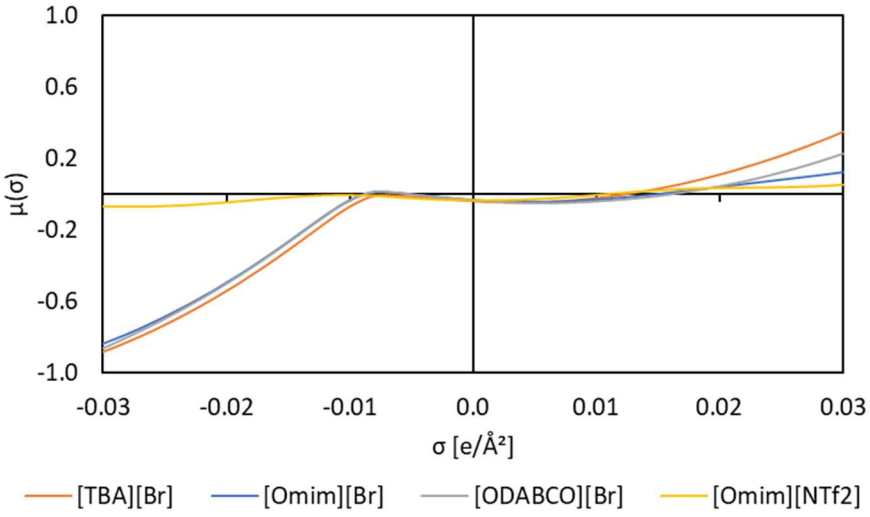


**Fig. S16**. $\sigma$-potentials of the ILs.

The potential $\mu(\sigma)$ can be viewed as the free energy needed for removing or creating screening charges, by breakage or formation of H-bonds. More specifically, if $\mu(\sigma) < 0$, a strong H-bond is formed, and the opposite holds for $\mu(\sigma) > 0$. Like with the σ-profile plot, the σ potential is divided into three main regions, namely the nonpolar region when $-0.0084$ e/Å$^2$ < σ < 0.0084 e/Å$^2$ (related to its ability to interact with nonpolar groups), the H-bond region when σ < − 0.0084 e/Å$^2$ (related to its ability to interact with hydrogen bond donors), and the H-bond acceptor region when σ > 0.0084 e/Å$^2$ (related to its ability to interact with hydrogen bond acceptors). Based on Fig. S15, MeOH and DMC can be likely to interact with nonpolar groups of the ILs due to the negative values in the nonpolar zone. Moreover, MeOH is more likely to interact with both H-bond donor and acceptor molecules because of highly negative value in the region of σ < − 0.0084 e/Å$^2$ and σ > 0.0084 e/Å$^2$. In addition

of exhibiting more negative in the nonpolar region, DMC also shows almost parabolic behaviour with positive value in the region of $\sigma > 0.0084$ e/Å$^2$, on the contrary, and will be slightly repelled by H-bond acceptor molecules and will be slightly attracted to H-bond donor molecules, although this effect is less pronounced for DMC than for MeOH. Therefore, it can be stated that the IL-affinity for DMC opposed to MeOH can be enhanced by giving the ILs a more non-polar character [6, 7]. Based on Fig. S16, the $\sigma$-potentials of the considered ILs are all quite similar in the region of $-0.0084$ e/Å$^2 < \sigma <$ 0.0084 e/Å$^2$ and $\sigma < -0.0084$ e/Å$^2$, except for the one from [Omim][NTf2]. The [Br]-anions cause the presence of screening charge densities outside of the non-polar region, which makes $\mu(\sigma)$ of the [Br]-ILs be closer to that of MeOH, suggesting the affinity among them. However, [TBA][Br] has a bulkier cation corresponding to the most negative peak in the non-polar region, implying those stronger intermolecular interactions between DMC and [TBA][Br] among [Br]-ILs. For [Omim][NTf2], it shows the lowest negative value in the region of $\sigma < -0.0084$ e/Å$^2$, which also explains its higher affinity towards DMC [6, 7]. Furthermore, all $\mu(\sigma)$ of [DMC] and ILs are positive in the region of $\sigma > 0.0084$ e/Å$^2$ while MeOH shows negative value in this region. As a result, there exists strong affinity between ILs and DMC, on the contrary, strong repulsive interaction between ILs and MeOH.

## References


1. Sharma, J. and S. Hashmi, *Plastic crystal-incorporated magnesium ion conducting gel polymer electrolyte for battery application.* Bulletin of Materials Science, 2018. **41**(6): p. 1-8.
2. Ali Ghumro, S., et al., *N-Alkylated 1, 4-Diazabicyclo [2.2. 2] octane–Polyethylene Glycol Melt as Deep Eutectic Solvent for the Synthesis of Fisher Indoles and 1 H-Tetrazoles.* ACS omega, 2017. **2**(6): p. 2891-2900.
3. Schottel, B.L., H.T. Chifotides, and K.R. Dunbar, *Anion-π interactions.* Chemical Society Reviews, 2008. **37**(1): p. 68-83.
4. Nikolaeva, D., et al., *Influence of ionic liquid-like cationic pendants composition in cellulose based polyelectrolytes on membrane-based CO2 separation.* Carbohydrate Polymers, 2021. **255**: p. 117375.
5. Blundell, R. and P. Licence, *Tuning cation–anion interactions in ionic liquids by changing the conformational flexibility of the cation.* Chemical Communications, 2014. **50**(81): p. 12080-12083.
6. Banerjee, T. and A. Khanna, *Infinite dilution activity coefficients for trihexyltetradecyl phosphonium ionic liquids: measurements and COSMO-RS prediction.* Journal of Chemical & Engineering Data, 2006. **51**(6): p. 2170-2177.
7. Matheswaran, P., et al., *Overview of activity coefficient of thiophene at infinite dilution in ionic liquids and their modeling using COSMO-RS.* Industrial & Engineering Chemistry Research, 2016. **55**(3): p. 788-797.